A98-31525 ICAS-98-2,9,4

NUMERICAL SHAPE OPTIMIZATION OF NATURAL LAMINAR FLOW BODIES

Th. Lutz* and S. Wagner†
Institute of Aerodynamics and Gasdynamics, University of Stuttgart
Stuttgart, Germany

Abstract

An efficient calculation method for viscous incompressible flow prediction about axisymmetric bodies has been coupled with a hybrid optimizer and an evolution strategy. The coupled tool was employed to perform numerical shape optimizations of natural laminar flow bodies for various Reynolds number regimes. Contrary to the usual approach, the body geometry is not optimized in a direct way with the present method. Instead, a source singularity distribution on the axis is used to model the body contour and the corresponding inviscid flow field. Viscous effects are considered by means of an integral boundary-layer procedure. The reliable and consistent transition prediction is of essential importance for a successful shape optimization of laminar bodies. Therefore, a proved e^n criterion is applied in the present investigations.

Nomenclature

A	amplitude of a Tollmien-Schlichting wave, field point
$c_{d\text{-}}$	drag coefficient
c_{d_V}	volumetric drag coefficient
c_f	skin friction coefficient
c_l	lift coefficient
c_p	pressure coefficient
D	body diameter, drag
f	frequency
H_{32}	shape factor
L	body length
n	amplification factor
Re	Reynolds number
Re_x	local Reynolds number
Re_L	Reynolds number based on body length
Re_V	volumetric Reynolds number
Re_{δ_1}	Reynolds number based on δ_1
s	arc length
Tu	turbulence level
U	velocity of the basic flow
U_e	velocity at the boundary-layer edge
U_∞	undisturbed freestream velocity
V	body volume
x, r	coordinates of the cylindrical system
α_i	amplification rate
α_r	wave number
δ_1	displacement thickness
Δx_i	length of the i^{th} source section
φ	eigenfunction
ν	kinematic viscosity
ρ	density of the fluid
ω	circular frequency
ω^*	dimensionless circular frequency

Indices

crit.	critical value
i	section number
I	value at the primary instability point
tra	transition point
V	quantity based on body volume

1 Introduction

Drag reduction by laminarization of the boundary layer plays an important role in aerodynamic aircraft design.[4] For example, the high performance of current sailplanes can only be obtained by extensive laminar flow regions on suction and pressure sides of the wing. With the application of laminar airfoil sections the drag contribution of the fuselage will achieve a significant amount.

For the aerodynamic design of three-dimensional fuselages with low skin-friction drag, laminar bodies of revolution are often used as a basis. Therefore, an important aerodynamic task is to find axisymmetric body shapes which show extensive laminar flow for a prescribed design Reynolds number range.

Theoretical and experimental investigations prove that for slender axisymmetric bodies with an almost flat pressure distribution only moderate local Reynolds numbers at the transition point can be achieved. Early Northrop flight tests[15] yield transition Reynolds numbers up to $Re_{x_{tra}} = 4.5 \cdot 10^6$ for an ellipsoid with a fineness ratio of $L/D = 9$.

*Research Assistant.
†Professor, Head of Institute, Member AIAA.

To increase $Re_{x_{tra}}$, the favourable pressure gradient in the forebody region has to be enlarged. This can be realized by reducing the fineness ratio. Such a body shape with a small length-to-diameter ratio was investigated by Carmichael[3] by means of drop tests carried out in the Pacific Ocean. For the examined Dolphin body with $L/D = 3.33$, a reduction of the volumetric drag coefficient of up to 60% could be achieved compared to turbulent standard torpedo shapes. This indicates the existence of extensive laminar flow regions for the investigated Reynolds number range up to $Re_L \approx 40 \cdot 10^6$. Further experimental research on natural laminar flow (NLF) bodies was conducted for example by Hansen & Hoyt.[17]

For the design of low-drag shapes both inverse calculation procedures as well as analysis methods coupled with optimization algorithms are generally used. Zedan et al.[40] applied an inverse potential method based on a doublet singularity distribution on the body axis coupled with an integral boundary-layer procedure. Numerical shape optimizations for the incompressible case were presented by Parsons et al.,[30] Dodbele et al.,[7] Coiro and Nicolosi[5] or Pinebrook,[31] for example. With the exception of Pinebrook, these authors employed direct analysis methods to calculate of the inviscid flow field. The potential methods are coupled with integral or finite-difference boundary-layer procedures to account for viscous effects. For the purpose of numerical shape optimization, high computational efficiency is required. Therefore, the displacement effect of the boundary-layer is usually neglected and empirical criteria are employed to determine the transition point.

As pointed out by various authors[5,7,9,40] the determination of the transition location by means of empirical criteria is the weakest link in the aerodynamic analysis of NLF geometries. Because the optimization process of laminar shapes is mainly influenced by the transition prediction, totally different geometries could result depending on the used criterion. For the shape optimizations presented in this paper, a semi-empirical e^n criterion based on linear stability theory was applied. The e^n method is expected to show more consistent results than empirical criteria. An indirect potential method is used to compute the outer flow, and an integral procedure serves for the calculation of the boundary-layer development. A hybrid optimizer as well as an evolution strategy were coupled with the aerodynamic model. The coupled tool was applied for the shape optimization of axisymmetric NLF bodies for a variety of design Reynolds number regimes. In this paper, the fundamentals of the optimization tool will be summarized. Furthermore, optimization results of body shapes with minimized volumetric drag coefficient will be presented. The problems connected with simplified prediction of laminar to turbulent transition are discussed in more detail.

2 Problems of Transition Prediction

Transition Process

Laminar to turbulent transition is a complex and yet not fully understood phenomenon. Basic transition research mostly deals with physical mechanisms occuring in two-dimensional, incompressible attached boundary layers under controlled conditions. It is assumed that natural transition is caused by similar mechanisms. Excellent and detailed descriptions of the present knowledge in boundary-layer transition are given for example by Arnal,[1] Kachanov[23] or Saric.[34] Here, only the most important phenomena are summarized.

At low freestream turbulence level sound or vorticity perturbations entering the boundary layer, are of small amplitude. In the region of the forward stagnation point the laminar boundary layer is stable against these disturbances, i. e. the perturbations are damped in that region. Downstream of the primary instability point, the basic flow becomes unstable against fluctuations and the amplitude of the disturbances grows in downstream direction.

When the disturbance amplitude exceeds a certain value, nonlinear interaction of 2D and oblique waves occurs. This secondary instability initiates the subsequent stages of the transition process. In the last stage, turbulent spots occur imbedded in the laminar basic flow. The size of the spots increases in downstream direction until they grow together and form a fully turbulent flow.

A correct theoretical calculation of the controlled transition process is only possible with direct numerical simulations[24,25,32] by solving the complete unsteady Navier-Stokes equations. Enormous computational effort is required for a single analysis.

Empirical Transition Criteria

In order to predict the onset of transition during the aerodynamic design process, a strongly simplified theoretical approach is needed. Because of their computational efficiency, empirical local criteria are often employed. These criteria represent correlations of integral boundary-layer parameters at the transition point. An overview of existing transition criteria is given for example by Arnal.[1]

As pointed out by Dodbele[8] empirical criteria are usually based on two-dimensional correlations for low Reynolds numbers and extrapolated to higher regimes. The scope of these empirical criteria is therefore expected to be limited. Several investigations demonstrate that a wide range of predicted transition locations can be found with different criteria.[37] This is

especially true for slender geometries with a flat pressure distribution.

Zedan et. al.[40] compared results obtained with the Michel e^n, the $H - R_x$, the Crabtree and the Granville criterion for the Hansen & Hoyt laminar body shape.[17] For $Re_V = 4 \cdot 10^6$ a transition location of $x_{tra}/L = 0.361$ was found with the Granville criterion. In contrast, no transition upstream of laminar separation at $x/L = 0.677$ was indicated by the Michel and the $H - R_x$ criterion. Such large discrepancies result in significant differencies with respect to the calculated drag coefficient.

Empirical criteria were also tested by Dodbele et. al.[7] to determine the transition point of the X-35 low-drag body. For $Re_L = 37.14 \cdot 10^6$ the examined criteria yield transition locations between $x_{tra}/L = 0.25$ and $x_{tra}/L = 0.68$, which corresponds to the laminar separation point. A linear stability analysis using the SALLY code was performed for comparison. Assuming a value of $n_{crit.} = 9$, transition onset was determined at $x_{tra}/L = 0.185$ according to the e^n method.

A further comparison of different transition criteria was reported by Coiro and Nicolosi.[5] The body of interest shows a long region with favourable pressure gradient and has been examined for $Re_L = 40 \cdot 10^6$. Again, a large discrepancy between different correlations results. The authors concluded that for accurate transition prediction a linear stability analysis should be performed. They also refer to the fact that such an analysis requires a lot of computational time and therefore may be impractical for the purpose of numerical optimizations. An alternative is offered in form of a data-base method as described in Section 3.3.

Linear Stability Theory

Semi-empirical transition criteria, such as the e^n method, consider the physics of the first transition stage. This first stage is characterized by an amplification of the Tollmien-Schlichting waves which can be calculated by means of the linear stability theory in very good agreement with experimental results.

Within linear stability theory the boundary-layer is separated into a steady basic flow and an unsteady disturbance. Furthermore, local parallelism is assumed. The basic flow represents a steady solution of the Navier-Stokes equation. A harmonic wave approach is chosen for the disturbance. Substitution of this approach into the complete Navier-Stokes equation, elimination of the pressure variable and linearization results in the well-known Orr-Sommerfeld equation. For two-dimensional flows, this equation can be expressed in the following form:[29]

$$\left(D^2 - \alpha^2\right)^2 \varphi = i\alpha Re \left[\left(U - \frac{\omega}{\alpha}\right)\left(D^2 - \alpha^2\right) - D^2 U\right] \varphi$$

$$\text{where} \quad D = \frac{d}{dy}$$

In the Orr-Sommerfeld equation, φ represents the complex amplitude function of the disturbance, being dependent on the wall normal distance y. In general, α and ω are complex and the above equation describes the growth of two-dimensional harmonic disturbance waves in time *and* space. If ω is introduced as a complex and α as a real quantity, only the time-dependent growth is considered. In contrast, spatial amplification is determined with a real circular frequency ω and a complex α. In the last case, the real part α_r represents the wavenumber and its imaginary part α_i the amplification rate. Negative values of α_i indicate a spatial amplification, whereas positive values mean decay of the perturbation wave amplitude. The instability depends on the disturbance frequency, the local Reynolds number and the boundary-layer profile.

Semi-empirical e^n Transition Criterion

The e^n criterion was independently developed by Smith & Gamberoni[36] and van Ingen.[21] With the e^n method it is assumed that the region of nonlinear amplification is short compared to the region of linear instability. In this case, linear stability theory can be applied to derive predictions about the onset of transition.

First, the development of the laminar boundary-layer has to be calculated. Then, a stability analysis must be performed by solving the Orr-Sommerfeld equation in the unstable region. This has to be done for different frequencies of the perturbation waves. Usually, no oblique waves are examined in the case of two-dimensional boundary-layers. For each disturbance frequency, the spatial amplification rates $\alpha_i(f)$ are integrated along the arc length s:

$$n(f) = \ln \frac{A(f)}{A_I(f)} = -\int_{s_I}^{s} \alpha_i(f) ds$$

The resulting amplification factor n represents the logarithmic ratio of the local disturbance amplitude A to the fictive amplitude A_I at the primary instability point.

With the e^n criterion, transition is assumed if the n-factor of the most amplified frequency reaches a certain critical value $n_{crit.}$. The corresponding location $s_{crit.}$ is determined by evaluating the envelope of the calculated amplification curves, see Fig. 1. The value of $n_{crit.}$ depends on the freestream conditions and the definition of the transition point (onset of transition or end of the intermittent region). Mack[28] and van Ingen[22] presented correlations for $n_{\text{crit.}}$ as a function of the freestream turbulence level.

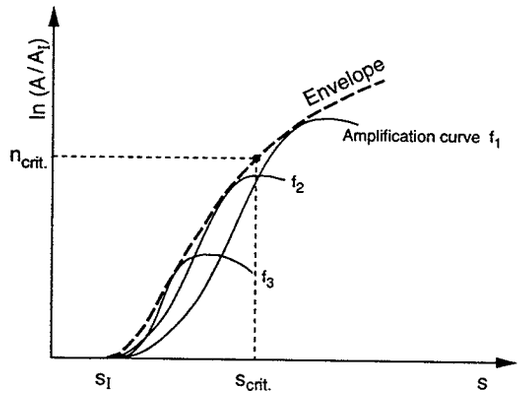

Figure 1: Principle of the e^n method

Note, that with the e^n method only an amplitude ratio of the disturbance waves is evaluated. The process of receptivity and the magnitude as well as the spectral distribution of the initial perturbation amplitude is not considered. The assumption of local parallelism and the neglection of nonlinear effects are further simplifications of the real transition process. Nevertheless, comparisons with transition experiments show that for two-dimensional boundary-layers the e^n approach yields better results than existing empirical criteria.[19,37] However, the method fails if large-amplitude perturbations enter the boundary layer and the linear stages of the transition process are bypassed.

The linear stability theory and the e^n method, as described, have been derived for an incompressible plane flow. Nevertheless, if the boundary-layer thickness is much smaller than the body radius, this approach can be applied for axisymmetric boundary layers as well.

e^n Envelope Method

A drastic reduction of the computational effort can be achieved with the e^n envelope method according to Gleyzes et. al.[14] and Drela.[10] With this approach the amplification curves of self-similar boundary-layer profiles are calculated in advance. The corresponding envelopes are approximated by straight lines and represented as a function of the shape factor. During actual transition calculations, these correlations are used to determine the n-factor.

Information about the dependency of the amplification on the perturbation frequency is lost with this simplified approach. It can be shown that a systematic error in the calculated n-factor results if a boundary layer with varying shape factor is examined.[6] This might be the reason why comparisons with transition experiments[37] show greater differences for the envelope approach than for the original e^n method.

3 Aerodynamic Model

3.1 Outer-Flow Computation

For the present investigations, potential-flow methods were used to calculate the inviscid flow field about axisymmetric bodies submerged in incompressible fluid.

To solve the direct problem, i. e. to calculate the velocity distribution for given geometries, a low-order panel method is applied. At zero incidence only the displacement effect of the body has to be considered. Therefore, it is sufficient to introduce a source distribution on the body surface. The singularity strengths are determined by application of the external Neumann boundary-condition at discrete collocation points. A modified Bézier spline is used to interpolate geometry and velocity distribution and provides the input data for the boundary-layer calculation. If required, the displacement effect of the attached boundary layer can be simulated by means of the transpiration technique. This necessitates an iterative procedure.

During the shape optimization process the inviscid flow field is calculated by means of an efficient indirect method based on a singularity distribution on the body axis. The present approach employs a source distribution varying linearly by section, as proposed by Zedan.[39] With a singularity distribution being specified, the corresponding potential and streamfunction values can easily be determined.[27] The velocity vector at an arbitrary field point results from differentiation of the streamfunction resp. the velocity potential. Because the body surface is identical to the stream surface, the defining equation for the contour is obtained by setting the streamfunction to the value at the stagnation points. The resulting equation has to be solved iteratively.

In order to generate body shapes of finite length, the closure condition has to be satisfied. This condition implies that the integral of the source strength has to be zero at the body tail. To avoid improper solutions, it is further neccessary to prevent negative values of the source strength integral within the singularity distribution.

Not all imaginable shapes can be modeled by means of a singularity distribution on the body axis. Geometries with small curvature radii in streamwise direction or bodies with a fineness ratio of $L/D < 1$ have to be excluded. It is assumed, however, that the relatively slender low-drag shapes can be generated with the indirect approach.

3.2 Boundary-Layer Method

A first-order integral procedure according to Eppler[11] is applied to calculate the boundary-layer development. This method was developed for the computation of incompressible attached boundary layers on

airfoil sections.[12] The approach is based on numerical integration of the integral momentum and energy equation. The laminar closure is derived from Falkner-Skan profiles in regions with adverse pressure gradient, whereas velocity profiles with suction are the basis in accelerated flow regimes. For turbulent boundary layers empirical relations are employed. The boundary-layer method has been expanded for the calculation of axisymmetric flows.

The empirical transition criterion used by Eppler has been replaced by a semi-empirical e^n method as described in the following section. In the present investigations, laminar separation bubbles are not considered. If laminar separation occurs upstream of transition, the method switches to turbulent closure conditions at the separation point.

The drag coefficient is determined using Young's formula,[38] which is based on the integral boundary-layer parameters at the body tail. With this formula, the skin friction as well as the form drag of the boundary-layer are considered. The equation of Young can be evaluated along the arc length s of the examined body. Depending on the boundary-layer method, different qualitative behaviour of the $c_d(s)$-curve can result, as discussed by Hess.[18] With the present integral procedure the maximum of the $c_d(s)$-distribution in the region of attached turbulent flow is attributed to represent the drag of the body. During the shape optimization process, a penalty function is introduced to account for the additional drag in case of turbulent separation.

3.3 Transition Prediction

The e^n criterion (see Section 2) is employed to determine the transition location with the analysis as well as the design method. In the present implementation, the amplification of 2D-waves in an incompressible basic flow is computed by direct solution of the Orr-Sommerfeld equation according to the spatial theory. The integration is performed by means of an iterative shooting method in combination with a classical Runge-Kutta scheme. A Gram-Schmidt orthonormalization is applied in order to enable a solution for high Reynolds numbers.

To perform a stability analysis, the boundary-layer profile and its first and second derivative are needed. However, with the employed boundary-layer procedure only integral parameters are calculated. Therefore, the required velocity profiles are determined from a polynomial approximation of the Falkner-Skan profiles. The shape factor H_{32} serves as a coupling parameter. As can be seen from Fig. 2 no significant differences with respect to the calculated amplification rates result from the approximation of the exact profiles.

For the family of the approximated Falkner-Skan profiles a non-ambiguous relation between the local

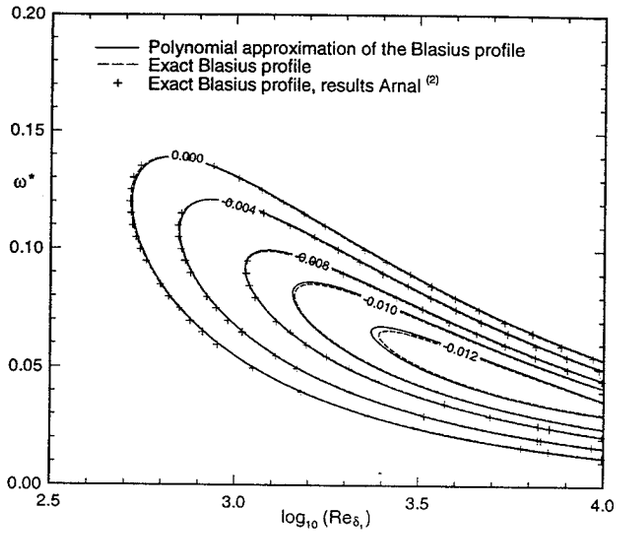

Figure 2: Stability diagram for the Blasius flow

Reynolds number and the shape factor at the primary instability point was established. Within actual transition calculations this correlation is used to determine the location of the instability point. Stability analysis then only has to be performed in the unstable region. This is done for a multitude of different physical perturbation frequencies at each coordinate point. To avoid superflous stability calculations, the analysed frequency spectrum is adjusted dynamically. This means that a specific frequency f is examined only if the amplification rate $\alpha_i(f)$ is negative or the total amplification factor $n(f)$ is greater than zero. Finally, the envelope is evaluated for the resulting amplification curves. Transition is assumed at the position where the envelope exceeds the specified value of $n_{\text{crit.}}$.

Transition prediction based on a direct solution of the Orr-Sommerfeld equation requires too much computational effort for the purpose of numerical shape optimization. For this reason, a database method was implemented, which can be used alternatively. To generate this database, the amplification rates α_i for 27 shape factors at 40 different Reynolds numbers and 40 different frequencies were calculated in advance. In order to enable the determination of a descend of the amplification curve, highly damped regions were also considered. During actual transition calculations the required value of α_i results from interpolation of database values. This simplified approach is robust and shows almost identical results compared to an exact calculation.

3.4 Validation Examples

The aerodynamic model has been verified with respect to drag prediction by comparison to experiments known from literature. For the case of forced transition

the water tunnel tests conducted by Gertler[13] constitute an excellent basis for the validation. Boundary-layer measurements with natural transition, however, are hardly known for axisymmetric bodies at high Reynolds numbers. An exception to this represent the experiments on a slender prolate ellipsoid ($L/D = 9$) as reported by Groth.[15] Fig. 3 shows the transition location vs Reynolds number as resulting from the corresponding F-94 in-flight tests. Good agreement is achieved with the present calculation method if a critical amplification factor between 9 and 11 is specified. This value of $n_{crit.}$ is lower than the one resulting from more recent in-flight tests[20] on a laminar glove of an aircraft wing ($n_{crit.} \approx 13.5$). The difference might be attributed to engine sound disturbances related to the F-94 flight tests. These disturbances cause an upstream shift of the transition location as noted by Dodbele.[7]

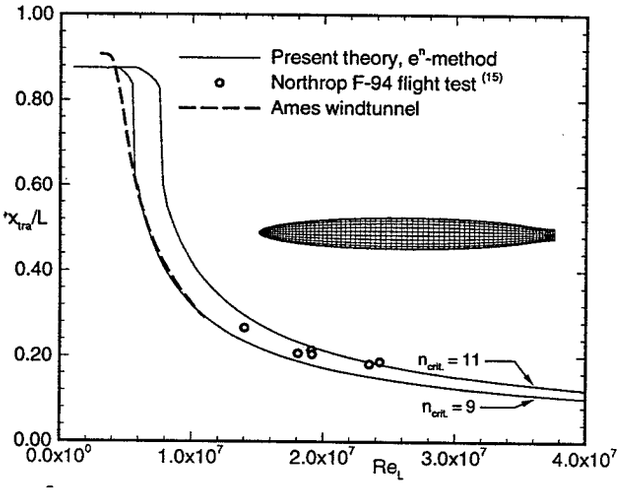

Figure 3: Transition location of the Northrop 1:9 ellipsoid (Exp. data taken from Carmichael[4])

Fig. 3 furthermore shows the experimental results obtained in the Ames low turbulence wind tunnel. The prediction is in good agreement for $n_{crit.} = 9$. Differences occur only for $Re_L < 5 \cdot 10^6$, which might result from the neglection of the boundary-layer displacement-effect within the present calculations.

As a further validation example, the calculated drag curve for the R 101 airship body is given in Fig. 4. In the 40's, experimental investigations for this shape were conducted independently by Jones and Schirmer.[35] Schirmer performed his measurements in the wind tunnel of the former Zeppelin company. For this tunnel, a turbulence factor of 1.35 is reported.[35] This corresponds to a turbulence level of $Tu \approx 0.45\%$ for which a critical amplification factor of $n_{crit.} = 5.7$ results from the correlation according to van Ingen.[22] The calculated drag curve for that value of $n_{crit.}$ shows satisfactory agreement with the experimental results.

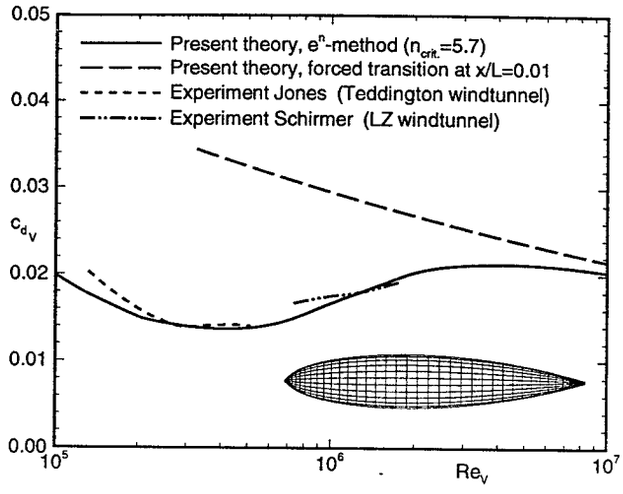

Figure 4: Drag curve for the R101 airship body

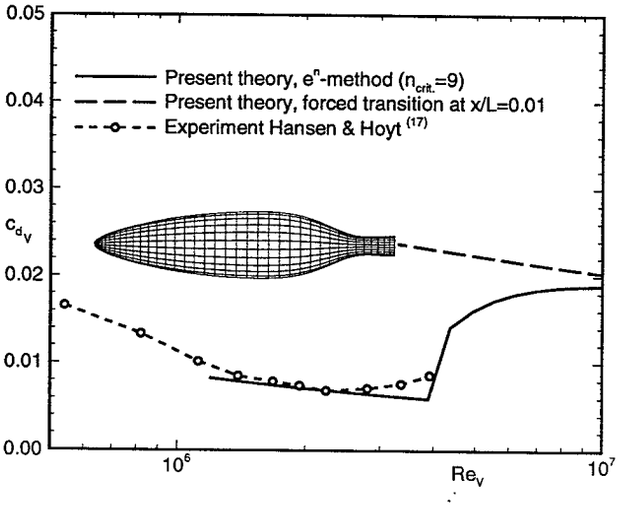

Figure 5: Drag curve for the Hansen & Hoyt body

Finally, the calculation results obtained for the laminar body of Hansen & Hoyt[17] are depicted in Fig. 5. The agreement found between computed and measured drag curve with natural transition is satisfactory. For $Re_V = 4 \cdot 10^6$ a drastic increase of the determined drag coefficient can be observed. This results from an abrupt upstream jump of the predicted transition location. The experiments show a more gradual drag rise. For the low Reynolds number regime laminar separation bubbles are indicated by the theory. The calculated drag curve is not plotted for this region since the bubble drag is not considered within the present aerodynamic model.

4 Optimization Procedure

The aerodynamic calculation method was coupled with different optimization algorithms in order to perform numerical shape optimizations of NLF bodies. The objective was to minimize the drag coefficient for a specified design Reynolds number regime. This optimization problem involves special requirements for the optimizer.

With the present aerodynamic model the gradient of the objective function (drag coefficient) cannot be determined analytically. Furthermore, it is expected that the objective function is multimodal, i. e. shows more than one minimum. As an additional difficulty, a complex topology of the objective function arises for bodies with maximized laminar flow regions: In the vicinity of the optimum, even smallest variations of the design variables can trigger an upstream jump of the predicted transition location. This leads to a drastic increase of the calculated drag coefficient, which corresponds to a jump of the objective function value. The optimization algorithm must therefore be efficiently applicable to such multi-dimensional, multimodal and nonlinear objective functions.

For the present investigations, a commercially available hybrid optimizer (POINTER) was applied. This tool enables constrained optimization and consists of a combination of genetic algorithm (GA), downhill simplex and a gradient method. A search procedure suitable for the optimization task at hand is chosen by means of automated training sessions with the desired optimization time being specified.

As a second optimization tool, an (1, 30)-evolution-strategy is employed. This optimization algorithm takes reference to the biological evolution process.[33] Mechanisms such as recombination, random mutation and selection are adopted to generate new design vectors from a given pool of inital designs. Of crucial importance for the success of an optimization process is the self-adaption of the step-size which is used for mutation of the design variables. For the present optimizations a covariance matrix adaption[16] was applied. With this method the mutation distribution is adjusted according to the selection information required along the entire evolution path.

The input parameters of the indirect potential method (see Sec. 3.1) are chosen as design variables to be varied by the optimizer. This approach is essentially similar to the one used by Pinebrook.[31] For the present examples, the lengths Δx_i of 20 source segments were optimized along with the corresponding singularity strengths at the section boundaries. In order to ensure a continous singularity distribution, the source strength at the end of each segment boundary is set equal to the value at the beginning of the following segment. A logarithmic scale has been introduced for Δx_i to prevent negative section lengths.

The source distribution as generated by the optimizer is superimposed by a parabolic correction distribution in such a way that the closure condition is fulfilled. An exact realization of that condition is necessary to enable the determination of the rear stagnation point. Negative values of the source-strength integral within the singularity distribution are avoided by using proper constraints during the optimization process.

5 Results and Discussion

As a first example, the shape optimization for a single design point is presented in order to illustrate the optimization process from a bad initial design to a low-drag shape. With this optimization, the objective was to minimize the drag D for a given body volume V and a prescribed airspeed U_∞. During the investigation of this question the following non-dimensionalized quantities have to be introduced:

$$c_{d_V} = \frac{D}{\frac{\varrho}{2} U_\infty^2 V^{2/3}}$$

$$Re_V = \frac{U_\infty V^{1/3}}{\nu}$$

In the first example, the volumetric drag coefficient c_{d_V} was chosen as objective function to be minimized for a volumetric Reynolds number of $Re_V = 1 \cdot 10^7$. The optimization was performed assuming natural transition with a value of $n_{crit.} = 9$ being specified for transition prediction. Because of the large number of restarts and different algorithms used, the hybrid optimizer is not well suited for the illustration of the optimization process. Therefore, the evolution strategy as described in the last section, was employed for this example. It should be noted that no geometric constraints were introduced. Therefore, the optimization process is driven solely by the aerodynamic objective to minimize drag.

The specified initial source distribution corresponds to an ellipsoid-like starting geometry with a fineness ratio of $L/D = 2.3$. Fig. 6 depicts the shape and the inviscid pressure distribution for this body as well as the skin-friction on the surface. The body shows early transition and furthermore turbulent flow separation which leads to a high drag coefficient.

At the beginning of the optimization process, designs with a pointed tail were selected (generation 40). Boundary-layer separation is prevented with these geometries. Then, the maximum thickness point is shifted downstream in order to delay transition (generation 500). Furthermore, a steep pressure recovery is introduced downstream of transition to reduce the wetted surface area and the skin-friction in the turbulent region.

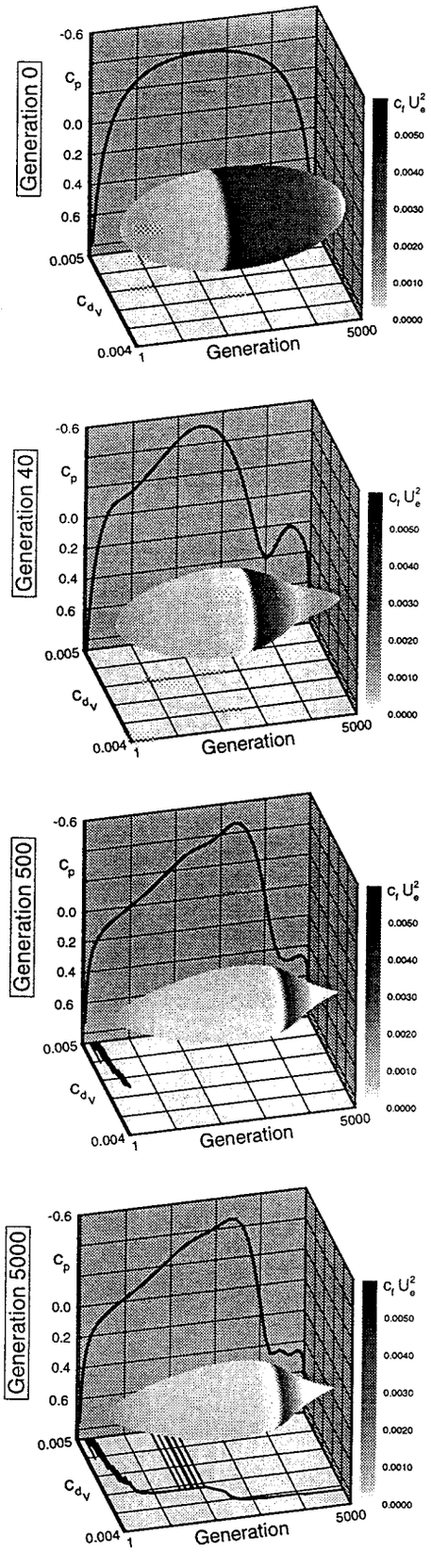

Figure 6: Optimization process of an axisymmetric body with minimized volumetric drag coefficient (Design point: $Re_V = 1 \cdot 10^7$)

Additionally, the development of the objective function value c_{d_V} is plotted in Fig. 6. A steep decrease can be observed within the first 500 generations. Then, no considerable improvement occurs up to generation 2000. Remarkable jumps of the c_{d_V}-value are obvious in that stage of the optimization process. Here, the laminar flow length is already maximized. Small geometry modifications in the forebody region result in a significant upstream jump of the predicted transition point and cause a drastic increase of the drag coefficient. At about generation 2500, the drag curve shows a steplike decrease. This indicates a successful adaption of the covariance matrix, which leads to a high convergence rate of the optimization process.[16]

Previous investigations[26] showed that one-point optimizations for a single Re_V lead to bodies which are inconvenient for practical application because they show bad characteristics outside the design point. This is especially true for laminar bodies at low Reynolds numbers. Therefore, NLF shapes for a whole Reynolds number range were optimized with the mean value of the drag coefficient c_{d_V} chosen as objective function.[27] This was done for five different design regimes (see table 1).

Table 1: Design regimes

Regime	$Re_{V_{min}}$	$Re_{V_{max}}$	$n_{crit.}$
I	$1 \cdot 10^6$	$3.16 \cdot 10^6$	9
II	$3.16 \cdot 10^6$	$1 \cdot 10^7$	9
III	$1 \cdot 10^7$	$3.16 \cdot 10^7$	9
IV	$3.16 \cdot 10^7$	$1 \cdot 10^8$	9
V	$1 \cdot 10^8$	$3.16 \cdot 10^8$	9

The starting geometry for design regime I corresponds to the ellipsoid-like shape as depicted in Fig. 6. First, an optimization run with the POINTER optimization tool was carried out. Thereafter, a further run with the evolution strategy was performed. This procedure was repeated for design regime II - V, taking the optimized geometry of the previous range as starting geometry. For each run with the evolution strategy, 10.000 generations were chosen which correspond to 300.000 designs with the employed (1, 30) strategy.

The resulting drag curves for all optimized body shapes are depicted in Fig. 7. These computations do not take the additional drag due to laminar separation bubbles into account. It can be seen that the bodies show a very low volumetric drag coefficient inside their respective design regimes. If the Reynolds number is increased slightly above the design region, an abrupt increase of the drag coefficient can be observed. This is caused by an upstream jump of the predicted transition point. Below the lowest design Reynolds number, laminar separation without reattachement is indicated. The drag curves are not plotted for this regime.

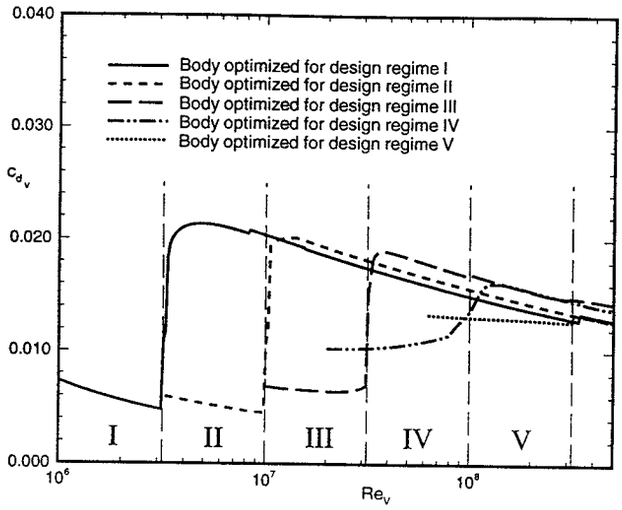

Figure 7: Drag curves of the optimized body shapes

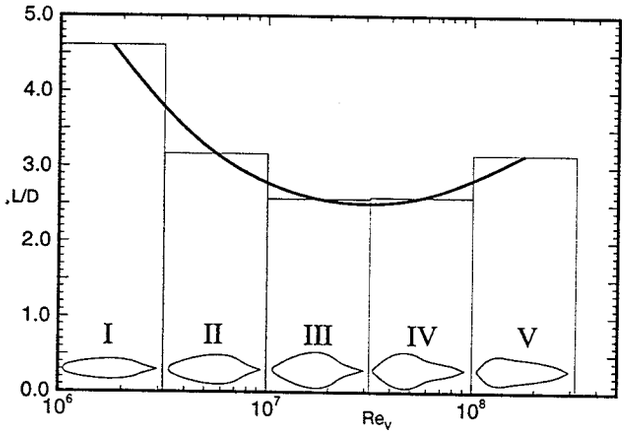

Figure 8: Fineness ratio of the optimized bodies

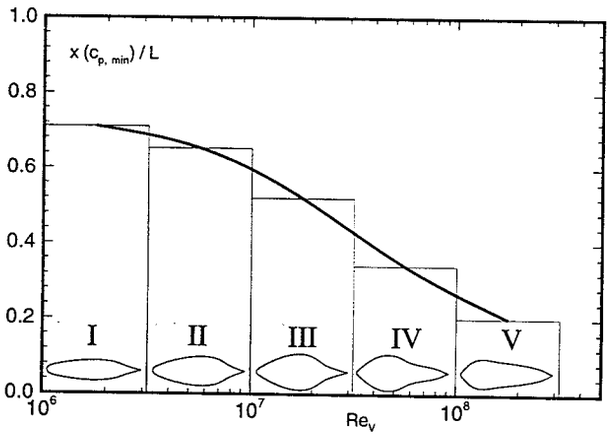

Figure 9: Minimum pressure position of the optimized body shapes

An evaluation of characteristic geometric parameters of the optimized shapes is given in Fig. 8 and 9. The body optimized for design regime I shows a relatively high fineness ratio ($L/D = 4.61$) and a far aft location of the minimum pressure coefficient. With increasing design Reynolds number the amount of favourable pressure gradient in the forebody region has to be enlarged in order to delay transition. This can be realized either by increasing the body diameter or by shifting the maximum thickness point upstream. However, enlarging the body diameter is limited by the maximum pressure recovery being possible without turbulent separation. Fig. 9 shows that for the optimized body shapes the $c_{p_{min}}$ location is shifted continously upstream with increasing design Reynolds number. In contrast to this, a minimum occurs in the curve of the fineness ratio. This indicates that for huge Reynolds numbers more slender geometries might be advantageous with respect to the volumetric drag coefficient. In other words, if the boundary layer is almost fully turbulent, body shapes with maximum pressure recovery do not represent an optimal solution.

As an example, the optimization result obtained for design regime III is presented in more detail. The contour and the inviscid pressure distribution of this body is depicted in Fig. 10. The body shows a steep favourable pressure gradient during the first 50% of its length. For the Reynolds number range considered, this is required to achieve extensive laminar flow by shaping alone.

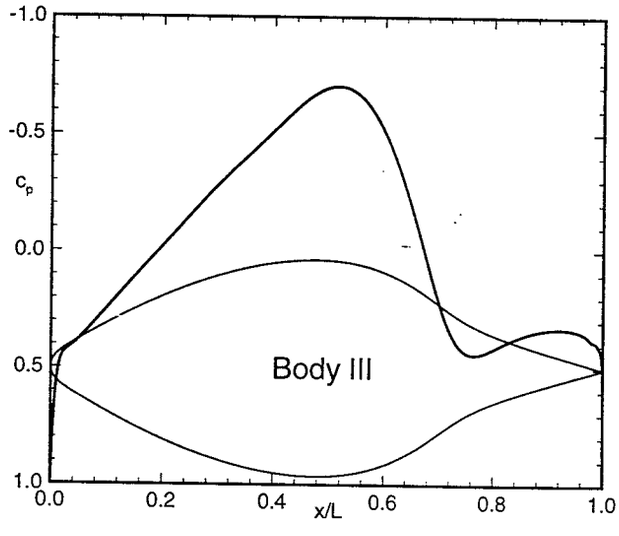

Figure 10: Shape and inviscid pressure distribution of the body optimized for design regime III

The amplification curves for the lowest and for the highest design Reynolds number are given in Fig. 11. Within this regime, the critical amplification factor is reached upstream of the laminar separation point. Therefore, no separation bubbles have to be expected. For $Re_V = 1 \cdot 10^7$ significant amplification occurs just at the beginning of the pressure recovery. In contrast,

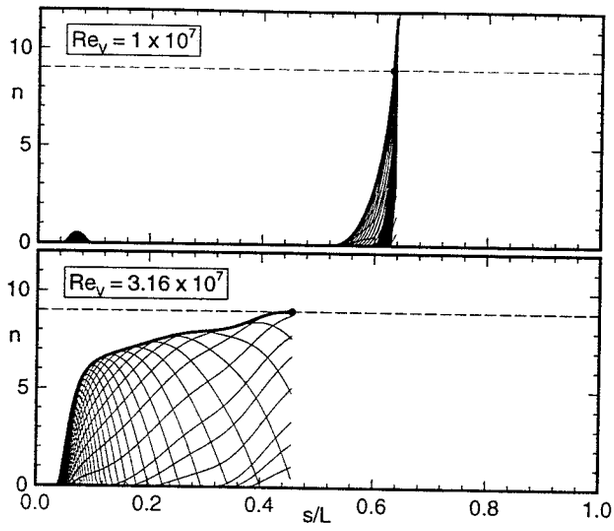

Figure 11: Amplification curves of body III

a strong disturbance growth in the nose region is determined for $Re_V = 3.16 \cdot 10^7$. An amplification factor of $n = 6$ is reached at an arc length position of $s/L = 0.09$. Downstream of this point the n-factor increases only gradually until transition is predicted at $s/L = 0.45$. An almost constant n-factor slightly below the critical value might result in nonlinear amplification in the real flow. If this is true, linear theory underpredicts the disturbance growth and a transition position too far downstream would be predicted with the e^n approach.

6 Conclusion

An efficient aerodynamic calculation method was developed and coupled with different optimization algorithms. In order to accurately predict the transition location, an semi-empirical e^n criterion is employed. The coupled tool was used for the numerical shape optimization of axisymmetric NLF bodies. The objective of the present investigations was to minimize the volumetric drag coefficient for different design Reynolds number regimes. No geometric constraints were introduced.

The resulting optimized body shapes show very low drag inside their respective design region. Slightly above the upper design Reynolds number, the calculated drag coefficient increases drastically. This results from an abrupt upstream jump of the predicted transition point in off-design conditions. Experimental validation of the optimized bodies has yet to be performed. Currently, measurements in a model basin are prepared. For these tests, a NLF body shape was especially optimized with regard to the onset flow conditions of the test facility.

References

[1] D. Arnal. *Description and Prediction of Transition in Two-Dimensional, Incompressible Flow.* AGARD AR 709, 1984.

[2] D. Arnal. *Diagrammes de stabilité des profils de couche limite auto-semblables, en écoulement bidimensionnel incompressible, sans et avec courant de retour.* Rapport Technique OA No 34/5018, 1986.

[3] B. H. Carmichael. *Underwater Drag Reduction Through Optimum Shape.* AIAA Second Propulsion Joint Specialist Conference, Colorado Springs, Colorado, June 13–17, 1966.

[4] B. H. Carmichael. *Personal Aircraft Drag Reduction.* Published by the author, 1996.

[5] D. P. Coiro and F. Nicolosi. *Design of Natural Laminar Flow Fuselages.* ICAS-94-4.7.4., 1994

[6] P. Dini, M. S. Selig, and M. D. Maughmer. *A simplified e^n method for separated boundary layers.* AIAA-91-3285, 1991.

[7] S. S. Dodbele, C. P. van Dam, P. M. H. W. Vijgen, and B. J. Holmes. *Shaping of Airplane Fuselages for Minimum Drag.* J. Aircraft, Vol. 24, No. 5, pp. 298–304, 1987.

[8] S. S. Dodbele. *Effects of Forebody Geometry on Subsonic Boundary-Layer Stability.* NASA Contractor Report 4314, 1990.

[9] S. S. Dodbele. *Design Optimization of Natural Laminar Flow Bodies in Compressible Flow.* J. Aircraft, Vol. 29, No. 3, May–June 1992.

[10] M. Drela and M. G. Giles. *Viscous-Inviscid Analysis of Transonic and Low Reynolds Number Airfoils.* AIAA-86-1786-CP, 1986.

[11] R. Eppler. *Praktische Berechnung laminarer und turbulenter Absaugegrenzschichten.* Ing. Archiv 32, pp 222–245, 1963; english translation: NASA TM–75328, 1987.

[12] R. Eppler and D. M. Somers. *A Computer Program for the Design and Analysis of Low-Speed Airfoils.* NASA TM 80210, 1980.

[13] M. Gertler. *Resistance Experiments on a Systematic Series of Streamlined Bodies of Revolution — for Application to the Design of High Speed Submarines.* Navy Department, Report C-297, Central Air Documents Office, Wright Patterson Air Force Base, Dayton, Ohio, April 1950.

[14] C. Gleyzes and J. Cousteix. *Theoretical and Experimental Study of Low Reynolds Number Transitional Separation Bubbles.* Proc. Conference on Low Reynolds Number Airfoil Aerodynamics, UNDAS-CP-77B123, Notre Dame, pp. 137–151, 1985.

[15] E. Groth. *Boundary Layer Transition on Bodies of Revolution.* Northrop Aircraft Rept. 57-1162 BLC-100, 1957.

[16] N. Hansen and A. Ostermeier. *Adapting arbitrary normal mutation distributions in evolution strategies: The covariance matrix adaption.* Proceedings of the 1996 IEEE International Conference on Evolutionary Computation, Nagoya, Japan, May 20–22, 1996.

[17] R. J. Hansen and J. G. Hoyt. *Laminar-To-Turbulent Transition on a Body of Revolution with an Extended Favorable Pressure Gradient Forebody.* Journal of Fluids Engineering, Vol. 106, pp. 202–210, June 1984.

[18] J. L. Hess and R. M. James. *On the problem of shaping an axisymmetric body to obtain low drag at large Reynolds numbers.* Douglas Aircraft Company, Long Beach, CA, Report MDC J6791, January 1975.

[19] B. F. A. van Hest. *Laminar-turbulent transition in boundary layers with adverse pressure gradient.* Dissertation, Delft University of Technology, 1996.

[20] K. H. Horstmann, A. Quast, and G. Redeker. *Flight and Wind-Tunnel Investigations on Boundary-Layer Transition.* J. Aircraft, Vol. 27, No. 2, 1990.

[21] J. L. van Ingen. *A Suggested Semi-Empirical Method for the Calculation of the Boundary Layer Transition Region.* Report Nos. V.T.H. 71, V.T.H. 74, Delft, 1956.

[22] J. L. van Ingen and L. M. M. Boermans. *Research on Laminar Separation Bubbles at Delft University of Technology in Relation to Low Reynolds Number Airfoil Aerodynamics.* Proc. of the Conference on Low Reynolds Number Airfoil Aerodynamics, Univ. of Notre Dame, pp. 89–124, 1985.

[23] Y. S. Kachanov. *Physical Mechanisms of Laminar-Boundary-Layer Transition.* Ann. Rev. Fluid Mech. 1994, pp. 411–482.

[24] L. Kleiser and T. A. Zang. *Numerical Simulation of Transition in Wall-Bounded Shear Flows.* Ann. Rev. Fluid Mech. 1991, pp. 495–537.

[25] M. Kloker. *A robust high-resolution split-type compact FD-scheme for spatial direct numerical simulation of boundary-layer transition.* Applied Scientific Research 58, Kluwer, 1998.

[26] Th. Lutz, H. Schweyher, S. Wagner, and R. Bannasch. *Shape Optimization of Axisymmetric Bodies in Incompressible Flow: Results for the High Reynolds Number Regime.* 2nd International Airship Conference, Stuttgart/Friedrichshafen, 3–4 July 1996.

[27] Th. Lutz and S. Wagner. *Drag Reduction and Shape Optimization of Airship Bodies.* To be published in J. Aircraft, 1998.

[28] L. M. Mack. *A numerical method for the prediction of high-speed boundary-layer transition using linear theory.* NASA SP-347, 1975.

[29] L. M. Mack. *Boundary Layer Linear Stability Theory.* AGARD-AR-709, 1984.

[30] J. S. Parsons and R. E. Goodson. *Shaping of Axisymmetric Bodies for Minimum Drag in Incompressible Flow.* J. Hydronautics, Vol. 8, No. 3, 1974.

[31] W. E. Pinebrook. *Drag Minimization on a Body of Revolution.* Dissertation at the Faculty of the Department of Mechanical Engineering of the University of Houston, 1982.

[32] U. Rist and H. Fasel. *Direct numerical simulation of controlled transition in a flat-plate boundary-layer.* J. Fluid Mech., Vol. 298, pp. 211–248, 1995.

[33] I. Rechenberg. *Evolutionsstrategie '94 - Werkstatt Bionik und Evolutionstechnik, Band 1.* Frommann-Holzboog Verlag, Stuttgart, 1994.

[34] W. S. Saric. *Physical Description of Boundary Layer Transition: Experimental Evidence.* AGARD-AR-793, 1994.

[35] M. Schirmer. *Aerodynamische Modellversuche an deutschen und ausländischen Luftschiff-Baumustern im Windkanal des Luftschiffbau Zeppelin in Friedrichshafen.* Dissertation, Technische Hochschule Carolo-Wilhelmina, Braunschweig, 1942.

[36] A. M. O. Smith and N. Gamberoni. *Transition, Pressure Gradient and Stability Theory.* Douglas Report No. ES 26388, 1956.

[37] W. Würz. *Hitzdrahtmessungen zum laminar-turbulenten Strömungsumschlag in anliegenden Grenzschichten und Ablöseblasen sowie Vergleich mit der linearen Stabilitätstheorie und empirischen Umschlagskriterien.* Dissertation, Institut für Aerodynamik und Gasdynamik, Universität Stuttgart, 1995.

[38] A. D. Young. *The calculation of total and skin friction drags of bodies of revolution at zero incidence.* ARC R&M No. 1874, 1939.

[39] M. F. Zedan and C. Dalton. *Potential Flow Around Axisymmetric Bodies: Direct and Inverse Problems.* AIAA Journal, Vol.16, No. 3, pp. 242–250, 1979.

[40] M. F. Zedan, A. A. Seif, and S. Al-Moufadi. *Drag reduction of airplane fuselages through shaping by the inverse method.* J. Aircraft, Vol. 31, No. 2, March–April 1994.

Lutz